3D image-domain wavefield tomography using time-lag extended images

Tongning Yang and Paul Sava, Center for Wave Phenomena, Colorado School of Mines*

SUMMARY

Image-domain wavefield tomography is a technique that reconstructs the velocity model by extracting information from migrated images. In time-lag extended images, velocity model accuracy can be evaluated by reflection focusing error, which represents the traveltime residual in the image domain. The model is updated by minimizing an objective function similar to the one used by wave-equation traveltime inversion. Unlike wave-equation traveltime inversion wherein traveltime residual is obtained from crosscorrelation of a single-shot data, the focusing error is extracted from time-lag gathers, which are wavefield crosscorrelations based on multiple experiments. Because the signal-to-noise ratio is higher in common-image gathers than that in common-shot gathers, our technique is able to measure focusing error more accurately in presence of noisy data and complex geologic structures. In addition, the image-domain approach is robust as it does not suffer from cycle-skipping, which is common in conventional data-domain full-waveform inversion. We illustrate the method using both synthetic and field data. The North Sea 3D field data example demonstrates that the technique is effective in optimizing the velocity model and improving image quality. In addition, the method is efficient in 3D because only the time-lag extensions are computed and stored.

INTRODUCTION

In seismic imaging, building an accurate and reliable velocity model remains one of the biggest challenges. The need for high-quality velocity models is driven by the wide spread use of advanced imaging techniques such as one-way wave-equation migration (WEM) and reverse-time migration (RTM) (Etgen et al., 2009).

In the past decade, velocity model building methods using full seismic wavefields (Vigh and Starr, 2008; Symes, 2009) become popular mainly due to their accuracy and to increased computational power.

One can divide the family of such velocity estimation techniques into data-domain methods (Sirgue and Pratt, 2004; Plessix, 2009) and image-domain methods (Sava and Biondi, 2004; Shen and Symes, 2008). Data-domain methods adjust the velocity model by minimizing the difference between simulated and recorded data (Tarantola, 1984; Pratt, 1999). This formulation is based on the strong assumption that the wave equation used for data simulation consists with the physics of the earth, which is often violated in practice. In addition, the methods also require low frequency data and sufficiently accurate initial model to avoid the cycle-skipping problem.

Unlike the data-domain approaches, image-domain methods update the velocity model by optimizing the image quality. As stated by the semblance principle (Al-Yahya, 1989; Yilmaz, 2001), the image coherence is optimized when the correct velocity model is used to migrate the data. The common practice is to optimize the coherency of reflection events in common-image gathers by updating the velocity model. In complex geology, image-domain wavefield tomography is capable of handling complicated wave propagation because it uses wave-equation engine to simulate the wavefields. Furthermore, the band-limited wavefields used in the velocity model building procedure are consistent with the wave-equation migration algorithms used in the areas.

Focusing analysis is a commonly used method for refining the velocity model (Faye and Jeannot, 1986). It evaluates the coherence of migrated images by measuring the focusing of reflections. Such information indicate the accuracy of the velocity model and thus can be used for model building (MacKay and Abma, 1992; Wang et al., 2005). For image-domain wavefield tomography, one can extract focusing information from time-lag extended images (Sava and Fomel, 2006).

Yang and Sava (2010a) analyze the relationship between the focusing error and velocity model accuracy, and develop a linearized wave-equation migration velocity analysis approach in 2D (Yang and Sava, 2010b). Here, we propose a methodology for 3D image-domain tomography also using the focusing information of migrated images. The essential idea is to extract focusing error from time-lag extended images, and then convert it into velocity updates. We explain the definition of the objective function and gradient computation in the theory section. Then we show the application of the method to a simple synthetic model and a North Sea 3D field dataset.

THEORY

The objective function for our wavefield tomography approach is

$$J = \frac{1}{2}\|\Delta\tau\|^2 \,. \tag{1}$$

Here $\Delta\tau$ stands for the focusing error which is defined as the distance where we observe a focus in time-lag extended images. Time-lag extended images are the crosscorrelation between extrapolated wavefields (u_s and u_r)

$$R(\mathbf{x},\tau) = \sum_j \sum_\omega \overline{u_s(j,\mathbf{x},\omega)} u_r(j,\mathbf{x},\omega)\, e^{-2i\omega\tau} \,. \tag{2}$$

The source and receiver wavefields u_s and u_r satisfy

$$\begin{bmatrix} \mathscr{L}(\mathbf{x},\omega,m) & 0 \\ 0 & \mathscr{L}^*(\mathbf{x},\omega,m) \end{bmatrix} \begin{bmatrix} u_s(j,\mathbf{x},\omega) \\ u_r(j,\mathbf{x},\omega) \end{bmatrix} = \begin{bmatrix} f_s(j,\mathbf{x},\omega) \\ f_r(j,\mathbf{x},\omega) \end{bmatrix} , \tag{3}$$

where $\mathscr{L}$ and $\mathscr{L}^*$ are forward and adjoint frequency-domain wave operators, f_s and f_r are the source and record data, j is the shot index, ω is the angular frequency, and $\mathbf{x}$ are the space coordinates $\{x,y,z\}$. The wave operator $\mathscr{L}$ and its adjoint $\mathscr{L}^*$ propagate the wavefields forward and backward in

time, respectively, using a two-way wave equation, i.e., $\mathscr{L} = -\omega^2 m - \Delta$, where m represent slowness squared and Δ is the Laplacian operator.

The objective function in equation 1 is the same as the one defined in wave-equation traveltime inversion (Luo and Schuster, 1991; Zhang and Wang, 2009). However, the physical meaning of $\Delta\tau$ in the objective functions is different. In our approach, $\Delta\tau$ is the focusing error measured from the stack of multiple-shots crosscorrelation. On the other hand, $\Delta\tau$ in wave-equation traveltime inversion is the traveltime misfit measure from a single-shot crosscorrelation.

After we define the objective function, we can compute the gradient using the adjoint-state method (Plessix, 2006). The first step is to construct state variables u_s and u_r, which relate the objective function to the model parameters (equation 3). The next step is to construct the adjoint sources, which are used to obtain adjoint-state variables. The adjoint sources are the derivative of the objective function with respect to the state variables. In our case, as $\Delta\tau$ is not directly dependent of the wavefields, we need to use the connective function developed by Luo and Schuster (1991). Since the focusing error represents the time lag when the reflection events focus, we have

$$R(\mathbf{x},\Delta\tau) = max\{R(\mathbf{x},\tau)\,|\,\tau\in[-T,T]\}\,. \tag{4}$$

As a result, the connective function can be written as

$$\begin{aligned}\dot{R}_{\Delta\tau} &= \left.\frac{\partial R}{\partial\tau}\right|_{\Delta\tau} \\ &= \sum_j\sum_\omega(-2i\omega)\,\overline{u_s(j,\mathbf{x},\omega)}u_r(j,\mathbf{x},\omega)\,e^{-2i\omega\Delta\tau}\,.\end{aligned} \tag{5}$$

The adjoint sources are then obtained as

$$\begin{aligned}g_s(j,\mathbf{x},\omega) &= \frac{\partial J}{\partial(u_s)} = \Delta\tau\frac{\partial(\Delta\tau)}{\partial(u_s)} \\ &= \Delta\tau\frac{\frac{\partial(\dot{R}_{\Delta\tau})}{\partial(u_s)}}{\frac{\partial(\dot{R}_{\Delta\tau})}{\partial(\Delta\tau)}} = \frac{\Delta\tau}{E}(2i\omega)\,\overline{u_r(j,\mathbf{x},\omega)}e^{2i\omega\Delta\tau}\end{aligned} \tag{6}$$

and

$$\begin{aligned}g_r(j,\mathbf{x},\omega) &= \frac{\partial J}{\partial(u_r)} = \Delta\tau\frac{\partial(\Delta\tau)}{\partial(u_r)} \\ &= \Delta\tau\frac{\frac{\partial(\dot{R}_{\Delta\tau})}{\partial(u_r)}}{\frac{\partial(\dot{R}_{\Delta\tau})}{\partial(\Delta\tau)}} = \frac{\Delta\tau}{E}(-2i\omega)\,u_s(j,\mathbf{x},\omega)\,e^{-2i\omega\Delta\tau}\,,\end{aligned} \tag{7}$$

where

$$E = \sum_j\sum_\omega 4\omega^2\overline{u_s(j,\mathbf{x},\omega)}u_r(j,\mathbf{x},\omega)\,e^{-2i\omega\Delta\tau}\,. \tag{8}$$

The adjoint-state variables are constructed similarly to state variables as follows:

$$\begin{bmatrix}\mathscr{L}^*(\mathbf{x},\omega,m) & 0\\ 0 & \mathscr{L}(\mathbf{x},\omega,m)\end{bmatrix}\begin{bmatrix}a_s(j,\mathbf{x},\omega)\\ a_r(j,\mathbf{x},\omega)\end{bmatrix} = \begin{bmatrix}g_s(j,\mathbf{x},\omega)\\ g_r(j,\mathbf{x},\omega)\end{bmatrix}. \tag{9}$$

The gradient is simply the crosscorrelation between state and adjoint-state variables:

$$\begin{aligned}&\frac{\partial J}{\partial m} = \\ &\sum_j\sum_\omega\frac{\partial\mathscr{L}}{\partial m}\left(u_s(j,\mathbf{x},\omega)\,\overline{a_s(j,\mathbf{x},\omega)} + u_r(j,\mathbf{x},\omega)\,\overline{a_r(j,\mathbf{x},\omega)}\right),\end{aligned} \tag{10}$$

where $\frac{\partial\mathscr{L}}{\partial m}$ is simply $-\omega^2$.

EXAMPLES

In this section, we first demonstrate the sensitivity kernel and gradient computation of our method using a simple synthetic model. Then, we show the application of the method to a North Sea 3D field dataset.

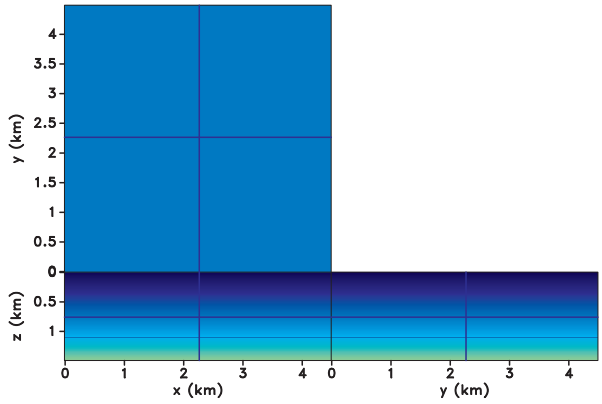

(a)

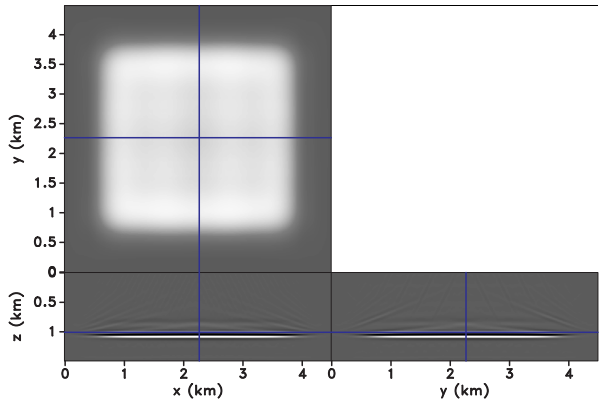

(b)

Figure 1: (a) The velocity model used for the inversion, and (b) the corresponding migrated image.

Figure 1(a) shows the velocity profile of the simple synthetic model. The model is a $v(z)$ with a velocity contrast located at $z = 1.1$ km to generate reflections. We simulate the data using acoustic two-way wave-equation finite-difference modeling. Next, we scale the true model by a factor 0.9 to construct the initial model and migrate the data to obtain the image and time-lag gathers. The migrated image is shown in Figure 1(b), and one can see that the reflector is mispositioned at

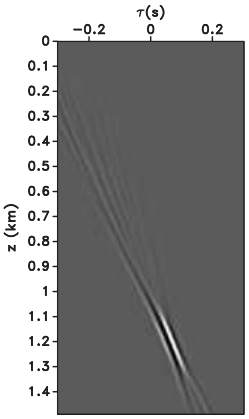

Figure 2: Time-lag gathers obtained with the initial model. The gather is located at at $x = 2.25$ km, $y = 2.25$ km.

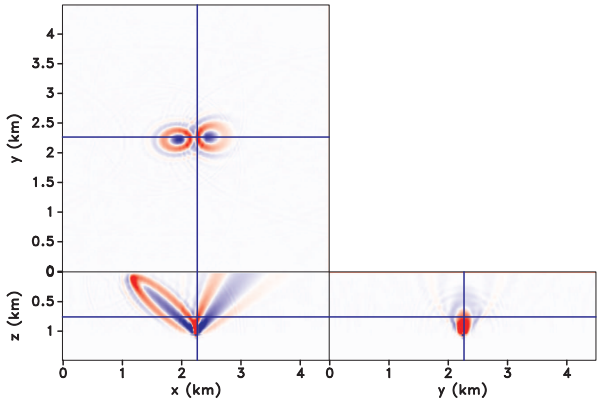

(a)

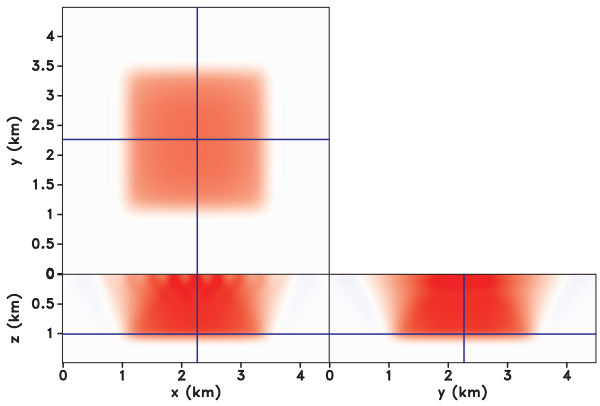

(b)

Figure 3: (a) The sensitivity kernel obtained with a single shot, and (b) the gradient obtained with all shots.

$z = 1.0$ km. Figure 2 show a gather located at the center of the model. As a wrong migration model is used, the reflection focus in the gathers is shifted to positive τ, indicating that the velocity is lower than the true model. Given the gathers, we can extract the focusing error $\Delta\tau$ by measuring the distance of the focus from zero τ. Figure 3(a) plots the sensitivity kernel obtained for one gather and one shot located at $x = 1.1$ km, $y = 2.25$ km, while Figure 3(b) plots the gradient obtained for all gathers and all shots. The gradient in red color is in negative value. This suggests that the velocity should be increased, which is consistent with the error in the initial model. Therefore, our method accurately captures the velocity error and correctly constructs the model update.

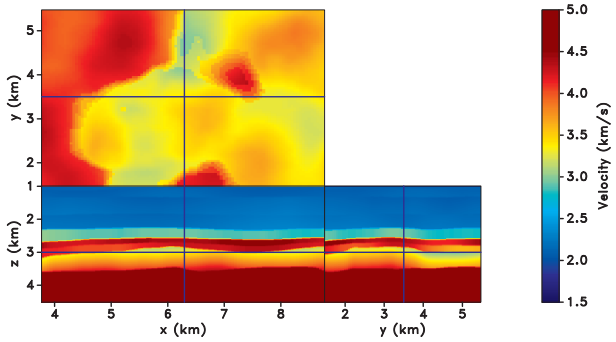

(a)

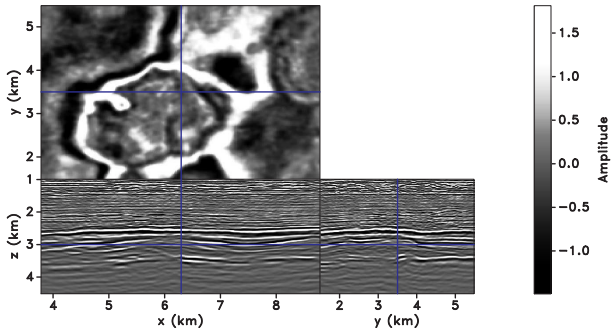

(b)

Figure 4: North Sea field data example. (a) The initial model used for the inversion and (b) the corresponding migrated image.

We also apply our method to a North Sea field dataset. The data are acquired in the Volve field and the construction of the anisotropic models (V_p, ε, and δ) are described in Szydlik et al. (2007). Here we assume that the medium is isotropic and use only the V_p model as the initial model to test our algorithm. Figure 4(a) and 4(b) show the initial model and corresponding migrated image. Using the objective function and gradient computation previously discussed, we run the inversion for five iterations. The updated velocity model and its corresponding migrated image are plotted in Figure 5(a) and 5(b). We can observe that the velocity is increased around the center part of the model after the inversion. This significantly improve the image quality, as the main reflections around $z = 2.8$ km are more focused and coherent. The continuity of the deeper reflections is improved as well. These improvements can be better observed in the zoom-in inline sections extracted at $y = 3.5$ km in Figures 6(a) and 6(b). To further assess the improvement due to the inversion, we also construct angle-domain common-image gathers before and after the inversion to evaluate the model accuracy. Figure 7(a)-7(b) and Figure 8(a)-8(b) plot the gathers sampled along in-line direction at three different cross-line locations using the initial and updated models, respectively. We notice that the main reflection around $z = 2.8$ km is character-

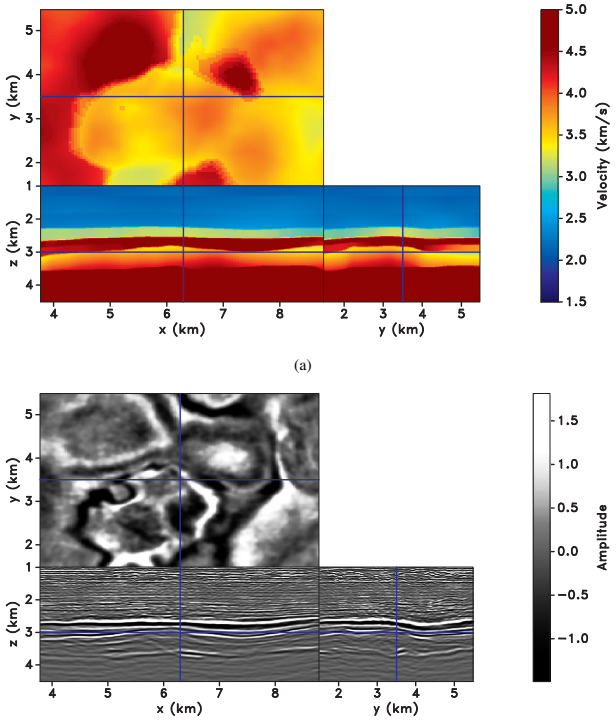

Figure 5: (a) The updated model obtained after the inversion, and (b) the corresponding migrated image.

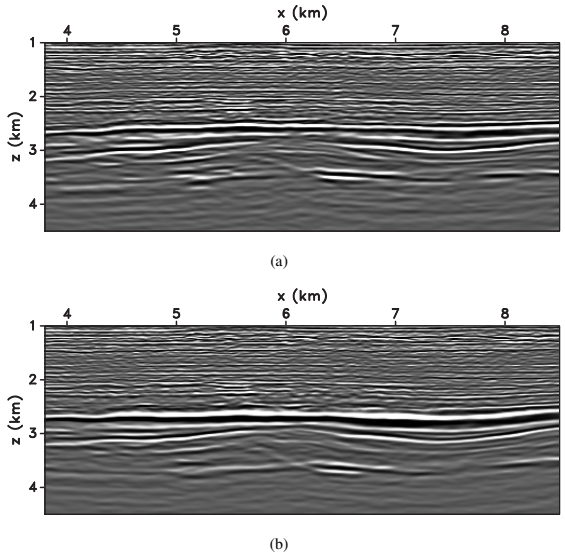

Figure 6: Zoom-in images obtained with (a) the initial model and (b) the updated model.

ized by flatter gathers after the inversion, which indicates the success of our method to improve the model accuracy.

CONCLUSIONS

We develop a 3D image-domain velocity model building technique based on time-lag extended images, which characterize

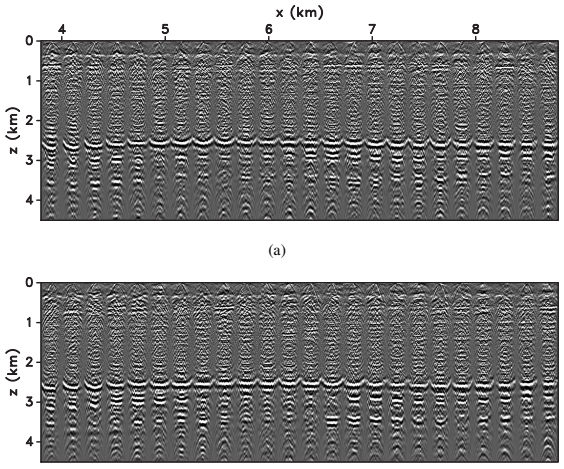

Figure 7: Angle-domain gathers obtained with the initial model at (a) $y = 3$ km and (b) $y = 6$ km.

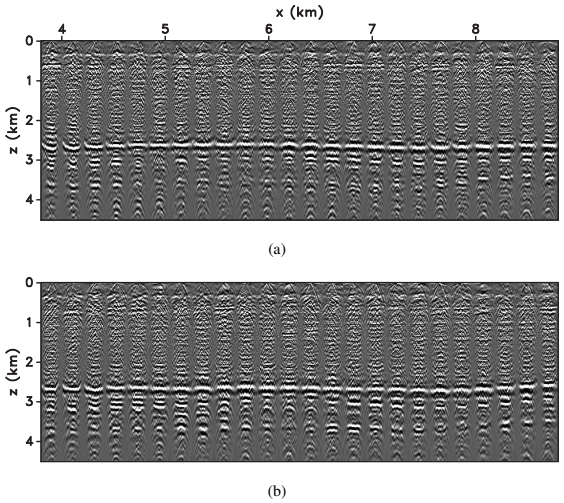

Figure 8: Angle-domain gathers obtained with the updated model at (a) $y = 3$ km and (b) $y = 6$ km.

the traveltime residual due to velocity error by reflection focusing. We formulate the optimization problem by minimizing the focusing error based on images constructed by wave-equation migration, which puts our technique in the family of wavefield tomography techniques. A North Sea field data example illustrates that our method is effective in improving model accuracy and image quality. In addition, the method is computationally efficient in 3D velocity model building applications.

ACKNOWLEDGMENTS

We thank sponsor companies of the Consortium Project on Seismic Inverse Methods for Complex Structures, whose support made this research possible. The authors would also like to thank Statoil ASA and the Volve license partners ExxonMobil E&P Norway and Bayerngas Norge, for the release of the Volve data.

REFERENCES

Al-Yahya, K., 1989, Velocity analysis by iterative profile migration: Geophysics, **54**, 718–729.

Etgen, J., S. H. Gray, and Y. Zhang, 2009, An overview of depth imaging in exploration geophysics: Geophysics, **74**, WCA5–WCA17.

Faye, J. P., and J. P. Jeannot, 1986, Prestack migration velocities from focusing depth analysis: 56th Annual International Meeting, SEG, Expanded Abstracts, 438–440.

Luo, Y., and G. Schuster, 1991, Wave equation traveltime inversion: Geophysics, **56**, 645–653.

MacKay, S., and R. Abma, 1992, Imaging and velocity estimation with depth-focusing analysis: Geophysics, **57**, 1608–1622.

Plessix, R.-E., 2006, A review of the adjoint state method for computing the gradient of a functional with geophysical applications: Geophysical Journal International, **167**, 495–503.

———, 2009, Three-dimensional frequency-domain full-waveform inversion with an iterative solver: Geophysics, **74**, WCC53–WCC61.

Pratt, R. G., 1999, Seismic waveform inversion in the frequency domain, Part 1: Theory and verification in a physical scale model: Geophysics, **64**, 888–901.

Sava, P., and B. Biondi, 2004, Wave-equation migration velocity analysis - I: Theory: Geophysical Prospecting, **52**, 593–606.

Sava, P., and S. Fomel, 2006, Time-shift imaging condition in seismic migration: Geophysics, **71**, S209–S217.

Shen, P., and W. W. Symes, 2008, Automatic velocity analysis via shot profile migration: Geophysics, **73**, VE49–VE59.

Sirgue, L., and R. Pratt, 2004, Efficient waveform inversion and imaging: A strategy for selecting temporal frequencies: Geophysics, **69**, 231–248.

Symes, W., 2009, Migration velocity analysis and waveform inversion: Geophysical Prospecting, **56**, 765–790.

Szydlik, T., P. Smith, S. Way, L. Aamodt, and C. Friedrich, 2007, 3d pp/ps prestack depth migration on the volve field: First break, **25**, 43–47.

Tarantola, A., 1984, Inversion of seismic reflection data in the acoustic approximation: Geophysics, **49**, 1259–1266.

Vigh, D., and E. W. Starr, 2008, 3D prestack plane-wave, full-waveform inversion: Geophysics, **73**, VE135–VE144.

Wang, B., F. Qin, V. Dirks, P. Guilaume, F. Audebert, and D. Epili, 2005, 3d finite angle tomography based on focusing analysis: 78th Annual International Meeting, SEG, Expanded Abstracts, 2546–2549.

Yang, T., and P. Sava, 2010a, Moveout analysis of wave-equation extended images: Geophysics, **75**, S151–S161.

———, 2010b, Wave-equation migration velocity analysis with time-lag imaging: Geophysical Prospecting, submitted for publication.

Yilmaz, O., 2001, Seismic Data Analysis (2nd edition): Society of Exploration Geophysicists.

Zhang, Y., and D. Wang, 2009, Traveltime information-based wave-equation inversion: Geophysics, **74**, WCC27–WCC36.